Geophysical Prospecting, 2004, **52**, 287–300

Unsupervised separation of seismic waves using the watershed algorithm on time-scale images

Antoine Roueff,* Jocelyn Chanussot, Jerome I. Mars and Minh-Quy Nguyen

Laboratoire des Image et des Signaux (LIS), UMR CNRS 5083, PO Box 46, 38402 Saint Martin d'Heres Cedex, France

Received November 2001, revision accepted February 2004

ABSTRACT

This paper illustrates the use of image processing techniques for separating seismic waves. Because of the non-stationarity of seismic signals, the continuous wavelet transform is more suitable than the conventional Fourier transforms for the representation, and thus the analysis, of seismic processes. It provides a 2D representation, called a scalogram, of a 1D signal where the seismic events are well localized and isolated. Supervised methods based on this time-scale representation have already been used to separate seismic events, but they require strong interactions with the geophysicist. This paper focuses on the use of the watershed algorithm to segment time-scale representations of seismic signals, which leads to an automatic estimation of the wavelet representation of each wave separately. The computation of the inverse wavelet transform then leads to the reconstruction of the different waves. This segmentation, tracked over the different traces of the seismic profile, enables an accurate separation of the different wavefields. This method has been successfully validated on several real data sets.

1 INTRODUCTION

The separation of the different waves of a seismic profile (see example in Fig. 1) is a common issue in seismic signal processing. It enables the extraction of the physical parameters in order to characterize each wave (propagation velocity, polarization, etc.) and improves the knowledge of the local constitution of the subsoil. In particular, this can be very interesting for petroleum firms which intend to study the subsoil. A large variety of methods already exists for the processing of geophysical signals: median filters, f–k pie-slice filters, eigenvector filters, etc. (Mari, Glangeaud and Coppens 1999; Mars, Rector and Lazaratos 1999). In our algorithm, the signal analysis is performed by the continuous wavelet transform (CWT). As shown by Chakraborty and Okaya (1995), the decomposition of the signal in the time-scale domain is convenient for the representation of the different events. Then, when the patterns of the waves are disjointed in this time-scale domain, the waves can be separated. Deighan and Watts (1997) showed that the surface waves could be similarly removed by the use of the discrete wavelet transform (DWT). The advantage of using the DWT is that it has a lower computational cost. However, the drawback of this transform is that, since the sampling of the time-scale image is minimal, the resolution of the image is low, and it is thus more difficult to define a boundary between the different waves. On the other hand, the CWT enables a better representation of the signal (with better resolution). This property allows us to use image processing possibilities (in particular the segmentation process). Thus, the separation process between the different waves can be done automatically (Roueff *et al.* 2001). Starting from a profile containing a large number of seismic events (Fig. 1), the algorithm isolates each wave propagation by producing new profiles, one for each detected wave, without any intervention by the geophysicist.

Section 2 describes the principle of the CWT used for this purpose. Isolating the different features of this time-scale representation (i.e. segmenting it) leads to the desired wave separation. We propose performing this segmentation automatically using the watershed algorithm (Vincent and Soille 1991).

*E-mail: antoine.roueff@lis.inpg.fr

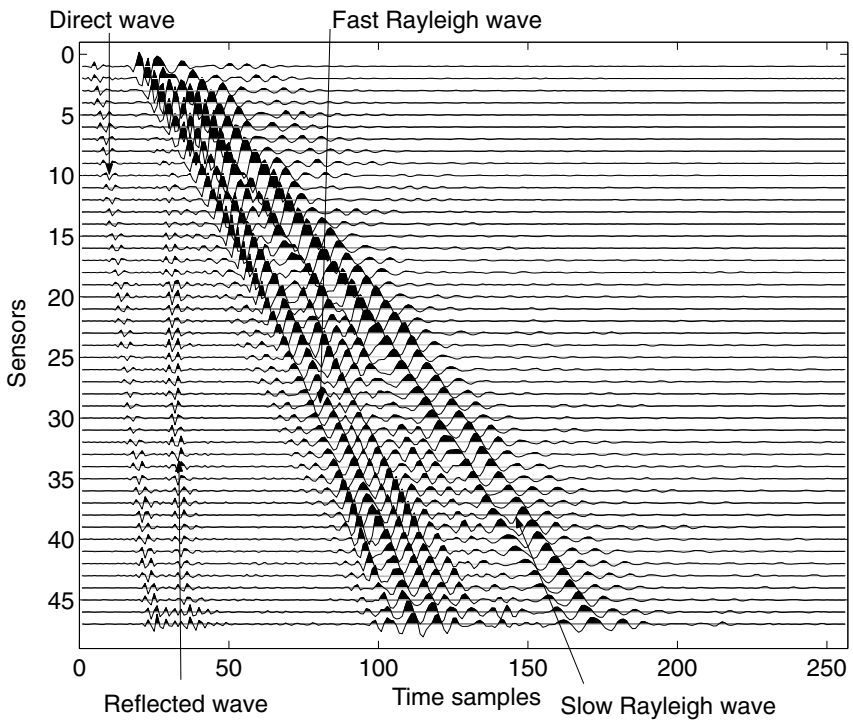

Figure 1 Real seismic profile recorded at Chantourne (France).

This is presented in section 3. Another key point of the paper is the tracking of the extracted features along the different sensors. Section 4 explains how the information redundancy provided by the spatial continuity along the sensors is exploited to initiate iteratively the segmentation of each image, avoiding the over-segmentation inherent in the watershed algorithm. Finally, results obtained using real data are presented in section 5.

2 CONTINUOUS WAVELET TRANSFORM

2.1 From the Fourier transform to the wavelet transform

The Fourier transform (FT) of a signal $f(t)$ is defined as

$$FT[f(t)](\omega) = \widehat{f}(\omega) = \int_{-\infty}^{\infty} f(t)\mathrm{e}^{-\mathrm{i}\omega t}\,\mathrm{d}t. \tag{1}$$

In the following, $f(t)$ represents a seismic trace and $\widehat{f}$ its Fourier transform. The FT estimates the harmonics that are present in the signal, by computing the correlation between $f(t)$ and $\mathrm{e}^{-\mathrm{i}\omega t}$ of t. Since the FT of $\mathrm{e}^{-\mathrm{i}\omega t}$ is a Dirac distribution, the harmonics are determined accurately in the spectral domain. But since the modulus of $\mathrm{e}^{-\mathrm{i}\omega t}$ is a constant, the FT gives no information about the time localization of these harmonics. Then, knowing that a seismic signal is the sum of transient waves, a trade-off is needed between a good localization in time (time representation) and a good localization in frequency (Fourier spectrum).

This can be achieved by windowing the Fourier transform to produce a better localization in time. This leads to the definition of the windowed Fourier transform (WFT) (Gabor 1946) or the short-time Fourier transform (STFT) (Nawad and Quatrieri 1988), whose definition is

$$WFT(f)(a,b) = \int_{-\infty}^{\infty} f(t)g(t-b)\mathrm{e}^{\mathrm{i}at}\,\mathrm{d}t, \tag{2}$$

where g is such that the energy of $g(t-b)\mathrm{e}^{\mathrm{i}at}$ is localized around b over an interval with standard deviation σ_t, where $\sigma_t^2 = \int t^2\|x(t)\|^2\,\mathrm{d}t$ (Papoulis 1977). In the frequency domain, the Fourier transform of $g(t-b)\mathrm{e}^{\mathrm{i}at}$ is localized around a over an interval of the standard deviation σ_ω, where $\sigma_\omega^2 = \int \omega^2\|\widehat{x}(\omega)\|^2\,\mathrm{d}\omega$ (Papoulis 1977). g is defined such that b is a translating factor in the time domain and a is a translating factor in the frequency domain. On the time–frequency plane, the energy boxes (i.e. localization of the energy) for time, FT and WFT representations are plotted in Figs 2(a), (b) and (c), respectively.

The Heisenberg inequality in signal processing gives the minimal bound for the area of these energy boxes:

$$\sigma_t\sigma_\omega \geq \frac{1}{2}. \tag{3}$$

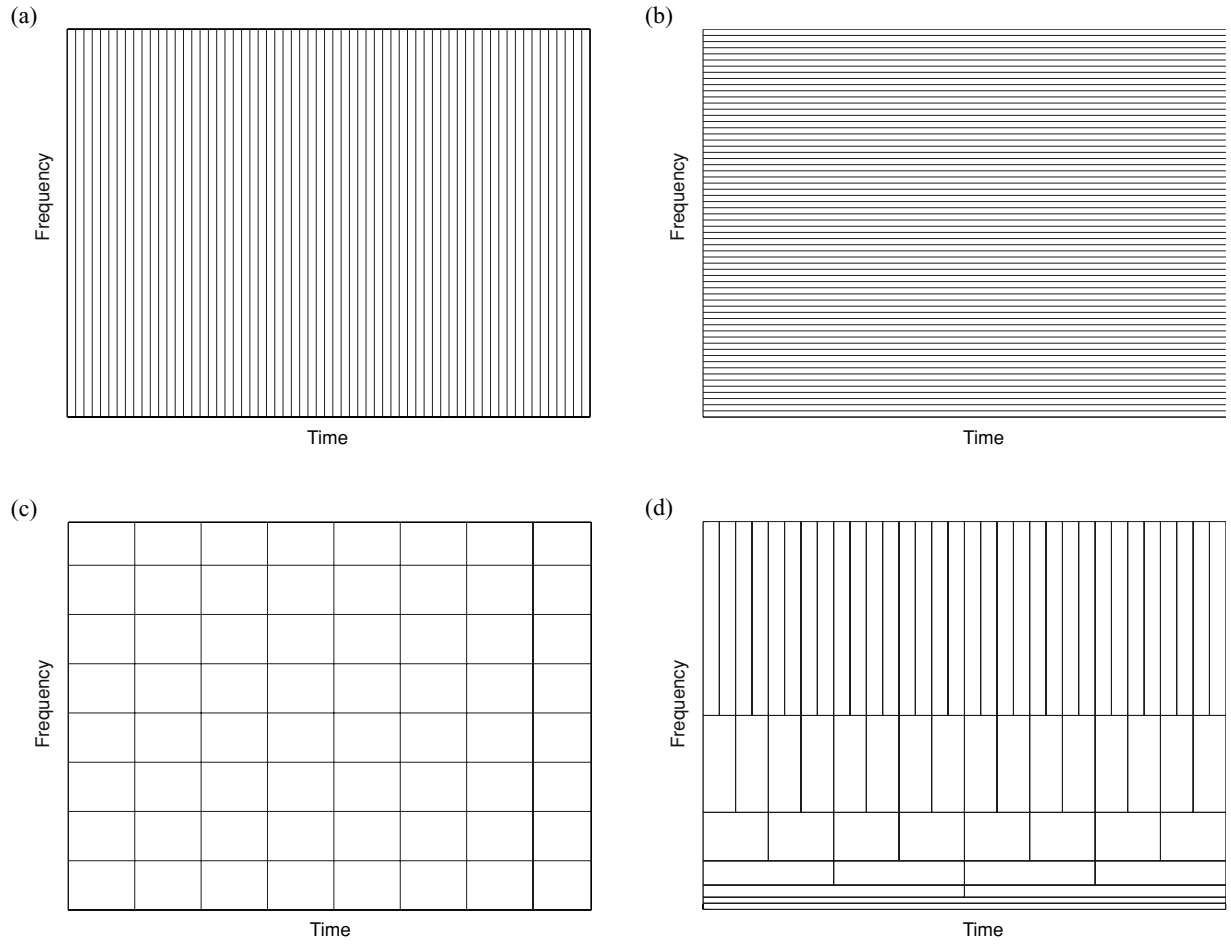

Figure 2 Different time–frequency representations: (a) natural time description, best localization in time, but no localization in frequency; (b) FT, best localization in frequency, but no localization in time; (c) WFT, good, and identical localization in time and in frequency everywhere in the time–frequency plane; (d) WT, good localization in frequency for low scales, and in time for high scales.

As explained by Chakraborty and Okaya (1995), in geophysics, a good localization in time is necessary to differentiate between high-frequency components, whereas for low-frequency components, a good accuracy in frequency is required. This means that, depending on their position in the time–frequency plane, the boxes should have different sizes. This is achieved by the wavelet transform (its representation in the time-scale plane is shown in Fig. 2(d)). Its definition is

$$CWT(f)(a,b) = \frac{1}{\sqrt{|a|}} \int_{-\infty}^{\infty} f(t)\psi\left(\frac{t-b}{a}\right)^{*} \mathrm{d}t, \qquad (4)$$

where $\psi(\frac{t-b}{a})$ (similarly to $g(t-b)\mathrm{e}^{\mathrm{i}at}$) is well localized around (b, a) in the time–frequency plane. In this case, b is still a translating factor in the time domain, but a is now a scaling factor in the frequency domain. Note that the wavelet $\psi(t)$ has the same shape for every a and b, but is contracted or dilated by the scaling factor a. In addition, $\psi_a(t) = \frac{1}{\sqrt{a}}\psi(\frac{t}{a})$ and $\widehat{\psi}_a = \sqrt{a}\psi(a\omega)$, which leads to $\sigma_{t\psi_a} = a\sigma_{t\psi}$ and $\sigma_{\omega\psi_a} = \frac{\sigma_{\omega\psi}}{a}$. This explains the organization of the boxes shown in Fig. 2(d). Note that there is no more information in $CWT(a, b)$ than in $f(t)$, but it gives a better representation in this case, where the different waves that are present are usually better separated.

For the implementation, many toolboxes are available on the Web (see
http://fractales.inria.fr/index.php?page=download_fraclab;
http://www-stat.stanford.edu/~wavelab/;
http://gdr-isis.org/Applications/tftb/iutsn.univ-nantes.fr/auger/tftb.html;
http://www.cmap.polytechnique.fr/~bacry/LastWave/).

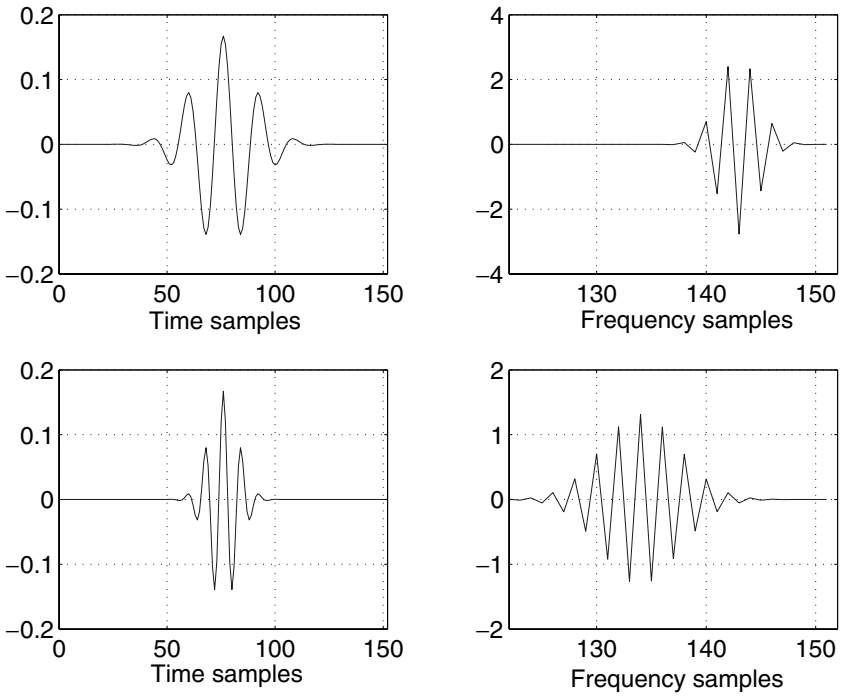

Figure 3 Time representation (left) and frequency representation (right) of the Morlet's wavelet (real part) at two different scales (upper and lower figures).

2.2 Morlet's wavelet

Various kinds of wavelet exist having different properties, e.g. localization, regularity, decay, symmetry (Abry 1997). The choice of the wavelet $\psi(t)$ depends on the application. In geophysics, Morlet's wavelet is the most widely used because of its many advantages. In particular, it has several interesting properties: it has exponential decay in time and frequency (i.e. good localization), it is infinitely derivable (i.e. quite regular) and it is symmetric (i.e. no phase distortion). In addition, its explicit definition leads to an easy implementation:

$$\psi(t) = (\pi t_0)^{-1/4} \exp\left[\frac{-1}{2}\left(\frac{t}{t_0}\right)^2 + 2i\pi f_0 t\right]. \qquad (5)$$

Moreover, its shape is very similar to a natural seismic wave; it is therefore very often used to recognize geophysical signals. Figure 3 shows the time and frequency representations of Morlet's wavelet at two different scales. Finally, because it is an analytic signal, computing the modulus of the complex coefficients leads to an amplitude representation where each wave is defined by a dome of energy (Chassande-Mottin 1998). Figure 4 shows one trace of the real seismic profile presented in Fig. 1, and the modulus of the corresponding wavelet transform. The modulus image clearly shows the presence of four localized regions in the time-scale plane: one for each of the dominant waves present in the trace. Note the correspondence between the time of appearance of the time representation and

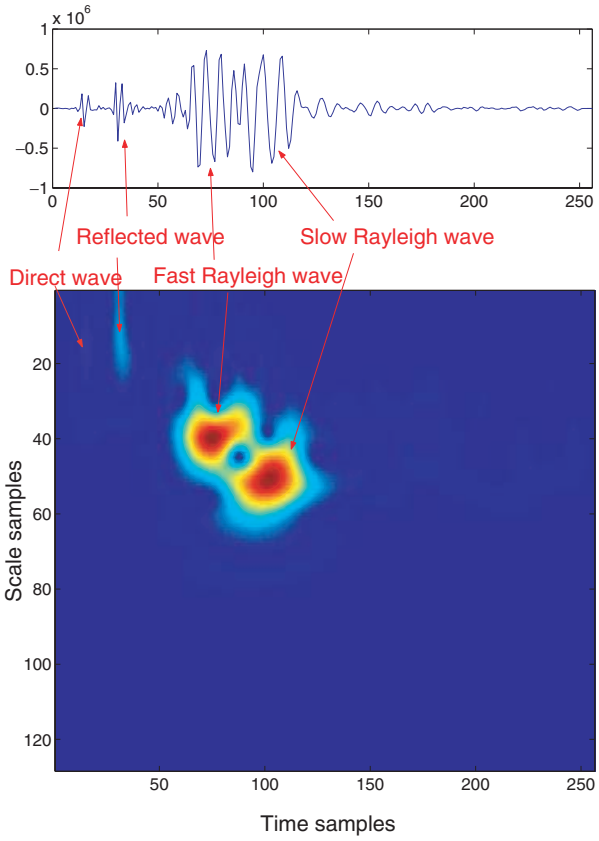

Figure 4 Time (upper) and time-scale (lower) representation (modulus) of a seismic trace.

of the (modulus) wavelet representation, and check the coherence of the corresponding scale:

- the direct wave at $b = 15$ and $a = 15$ (small scale corresponding to a high frequency),
- the reflected wave at $b = 30$ and $a = 15$,
- the fast Rayleigh at $b = 75$ and $a = 40$,
- the slow Rayleigh at $b = 100$ and $a = 50$.

Our purpose is to isolate automatically these four dominant waves.

2.3 Filtering in the time-scale plane

There are different ways to filter the time-scale plane. A review of different methods in time–frequency has been presented by Kozek and Hlawatsch (1992). We chose the masking method, since it has a low calculation cost and is simple to use. The time-scale representation can be processed as an image where each feature corresponds to a given wave. Using a manually set masking, Nguyen, Glangeaud and Mars (1999) isolated the different features of the image. Figure 5 shows this separation process on one trace: firstly the wavelet transform of the signal is computed, then the feature corresponding to the fast Rayleigh wave is extracted by segmentation and masking, and finally, the inverse wavelet transform (IWT) of the isolated feature is computed, leading to the reconstruction of the desired wave. Of course, this process can be applied to each feature of the time-scale representation (i.e. to each wave). In this example, the wave has been well isolated. Comparing the initial trace with the isolated trace (Fig. 6), the error is small. In addition, it should be noted that the extraction is better than it would be by a classical manual (time) muting process.

Since the wavelet is complex, in order to compute the IWT, the phase should also be estimated. Let us take a pixel (a, b) of the estimated complex wavelet. There are two cases:

- If (a, b) is in the region where the estimated modulus is non-zero (i.e. in the region of the estimated wave), then the phase

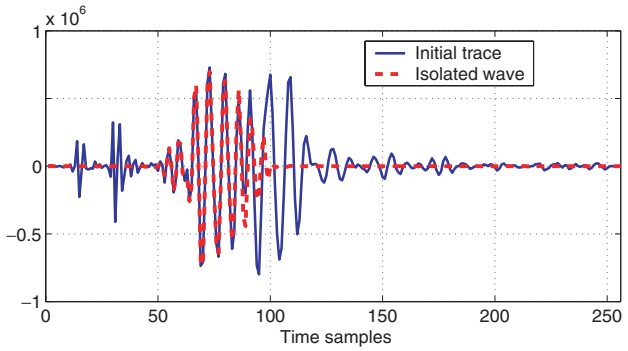

Figure 6 Evaluation of the reconstructed Rayleigh wave.

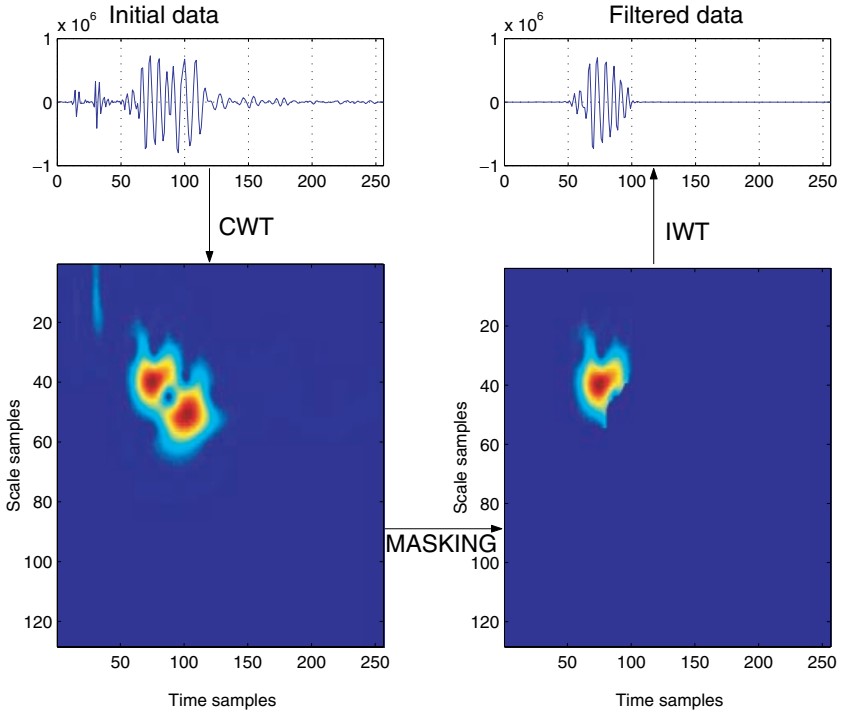

Figure 5 Separation and reconstruction of the fast Rayleigh wave.

value of this pixel should be the same as the phase value of the $CWT(f)(a, b)$. The phase has to be left unchanged for these pixels.

- If (a, b) is in the region where the estimated modulus is zero, then the phase value should be different, but since the modulus is zero, the phase value is of no consequence.

In conclusion, the phase is left unchanged everywhere. The assumption of this step is that the wave is well isolated from the other waves on the modulus image. The computation of the IWT has been detailed by Daubechies (1992). Its definition is given by

$$f(t) = \frac{1}{C_\psi} \int_{b\in\mathbf{R}} \int_{a>0} CWT(f)(a, b) \frac{1}{\sqrt{a}} \psi\left(\frac{t-b}{a}\right) \mathrm{d}b \frac{\mathrm{d}a}{a^2}, \quad (6)$$

where

$$C_\psi = \int_0^\infty \frac{\|\widehat{\psi}(\omega)\|^2}{\omega} \mathrm{d}\omega. \quad (7)$$

In addition, to check the accuracy of the result, we compare the CWT of the reconstructed trace with the CWT of the initial trace (Fig. 7). The shape of the modulus of the reconstructed wave is similar to the initial one in the zone of the reconstructed wave, which means that the reconstructed wave is correct. After the validation of the work of Nguyen (2000), we decided to automate the process by finding a segmentation algorithm able to perform the feature extraction in the time-scale domain automatically.

3 SEGMENTATION ALGORITHM

3.1 Watershed algorithm

Each seismic wave corresponds to a local maximum of the time-scale (modulus) representation of the seismic signal. The segmentation of the time-scale image leads to the extraction of the feature and thus to the wave separation. Among the numerous techniques proposed in the image processing literature, the watershed algorithm (Vincent and Soille 1991) is the most suited to the problem addressed in this paper (Pierson and Martin 1995). It basically consists of grouping pixels that are connected to the same local maxima. Unlike all the other classical segmentation techniques (Parker 1997), it allows us to aggregate pixels that have very different values in the same region (assuming they are connected to the same local maximum). Actually, the segmentation process can be seen as a merging process if we consider the negative image. For illustration purposes, this merging process of the algorithm is illustrated on a one-dimensional curve shown in Fig. 8. Imagine that some holes are dug at the local minima of the curve. These points are called the 'seeds'. Now assume that the curve is progressively immersed in water. The different regions, defined by the different seeds, expand progressively by aggregating surrounding points with increasing values, and when two regions tend to become connected to each other, a dam is built to keep them separated. At the end of the process, the different regions are isolated one from

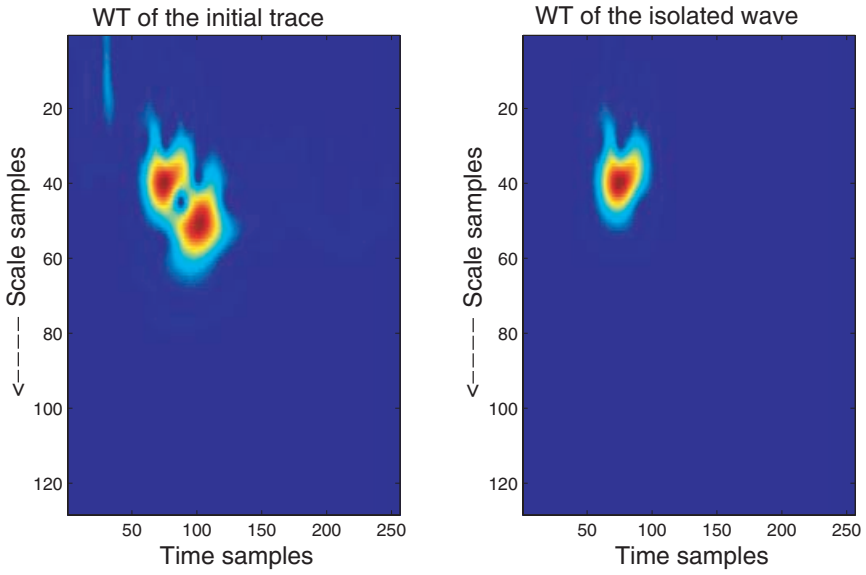

Figure 7 Separation and reconstruction of the fast Rayleigh wave.

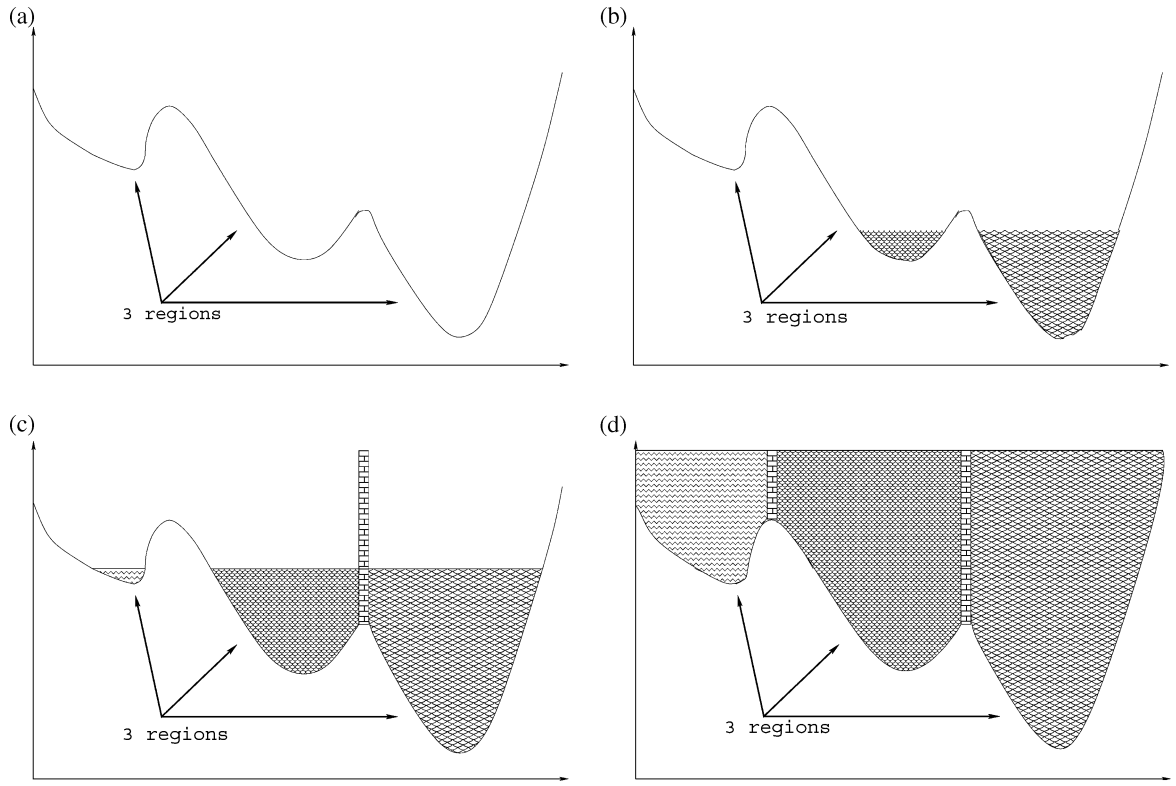

Figure 8 The four steps in the merging process of the watershed algorithm. (a) Start of the process, (b) 1/3 of the process, (c) 2/3 of the process, (d) end of the process.

each other by the 'dam network', which is also called the watershed.

This basic presentation of the separation process in 1D can be generalized in 2D. Now, referring to Fig. 4, by reversing its amplitude (i.e. red becomes the smallest amplitude), each region characterizing a wave can be seen as a catchment basin. By setting the seeds at the local minima of this negative image and then applying the watershed algorithm, it is possible to separate the different regions (i.e. the different waves).

3.2 Design of the algorithm

In our application, the number of desired regions can be predetermined. Assuming that the number of waves, n, and the locations of their seeds are known (section 4 gives details of the way the seeds are chosen), the number of regions (also called labels) is set at $n + 1$, i.e. one label for each wave and one more for the background of the modulus image. The good localization of the different-energy waves enables the definition of the background region, which contains all the information not relevant to the reconstruction of the energy waves. This is typically the noisy part of the signal, but it can also include some weak-energy waves.

In fact, the background region is often the biggest region (in terms of area). Then, to speed up the merging, the background region is firstly roughly estimated by a thresholding of 1% of the maximum. This threshold value is a trade-off between the acceleration of the algorithm and the loss of information about one of the waves we want to isolate. Referring to Fig. 9, a simple threshold is applied to the first image to get a binary image (the second image). A geodesic reconstruction (Serra 1988) is then performed so that all the brown regions that are not connected to the border of the image are suppressed (the third image). Finally, the estimated background is set at zero, and the rest of the image is inverted (to enable the merging process).

$\mathbf{L}$ is the matrix which defines the label value of each pixel. At the beginning of the process, all the pixels which are known to belong to the background are labelled 1, and the pixels of the seeds are labelled 2, 3, 4, ..., $n + 1$, according to region. Note that the number of regions that will divide the image is

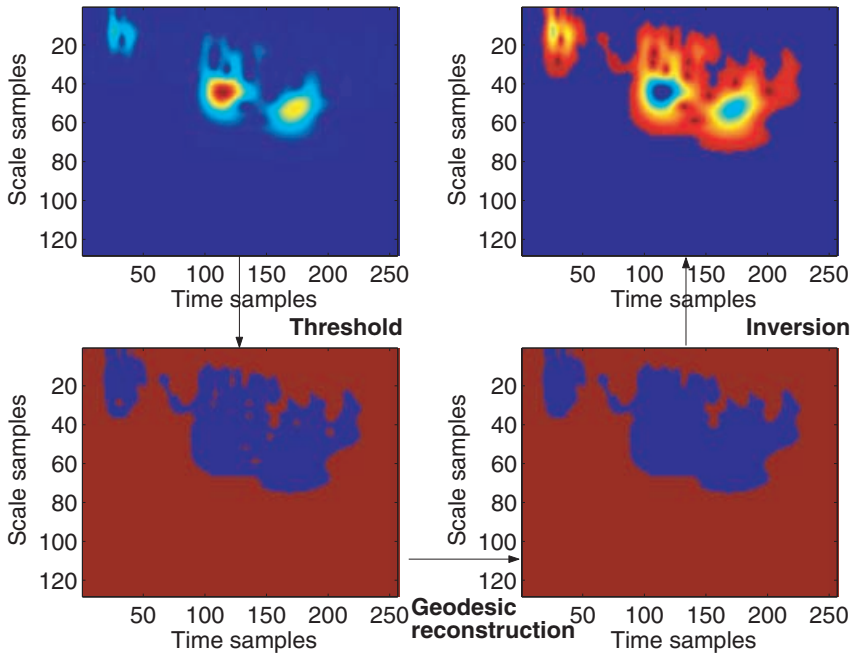

Figure 9 Thresholding of the data.

fixed by the seeds: a wave will be segmented if, and only if, it has an associated seed, which will initialize the increase of the corresponding region.

We then have to handle the situation when a wave has no seed. This case is illustrated in Fig. 10. On the first image, which is a zoom of the **L** image at the step t_0 during the merging process:

- green pixels label the background,
- orange pixels label the fast Rayleigh wave,
- yellow pixels label the slow Rayleigh wave,
- light blue pixels are unmerged,
- dark blue indicates pixels which would have been labelled (i.e. merged) if they had initially been connected to a labelled pixel.

These dark blue pixels represent a basin in the modulus image which has no seed. It represents a zone where there is an unexpected air wave (see the last image). As geophysicists, we do not wish to label this wave. It should not be merged in the region of the fast Rayleigh wave. The criterion for rejecting pixels to the background is that dark blue pixels should be weaker (in amplitude) in the modulus image than the pixels which link the two regions. The algorithm will then assume that those merged but unlabelled pixels should be rejected to the background image. It can be seen on the image that all the lower pixels are rejected in the background, and at the end of the process, the region is well designed.

3.3 Suppression of meaningless seeds

Considering the initial module image, the local maxima will be rejected in the background label. It is desirable to remove the small basins due to the presence of an unexpected wave. In the same way, in the case of noisy data, a lot of meaningless local maxima have to be removed. This is achieved using a suitable preprocessing procedure: the modulus image is filtered with a levelling transform called the hmax transform (Serra 1988). This operation consists of 'filling up' the maxima that have a local range smaller than a given threshold $h_{\max}$. In fact, it performs a geodesic reconstruction of the module image decreased by the amplitude hmax in the initial image. A one-dimensional illustration of this transform is presented in Fig. 11.

As a result, all the 'small' maxima due to the noise are removed. The remaining maxima represent some basins which detect the presence of existing waves (like the four waves previously discussed, but also like the air wave of Fig. 10). So the value of the $h_{\max}$ parameter has to be high enough to get rid of the irrelevant seeds, and small enough not to lose any true wave frontier. In practice, since the data contain little noise, we chose $h_{\max} = 1\%$ of the maximum value.

Using this segmentation algorithm, we automatized the separation process in 2D in the time-scale plane. In the next section, the unsupervised extension of the method to three

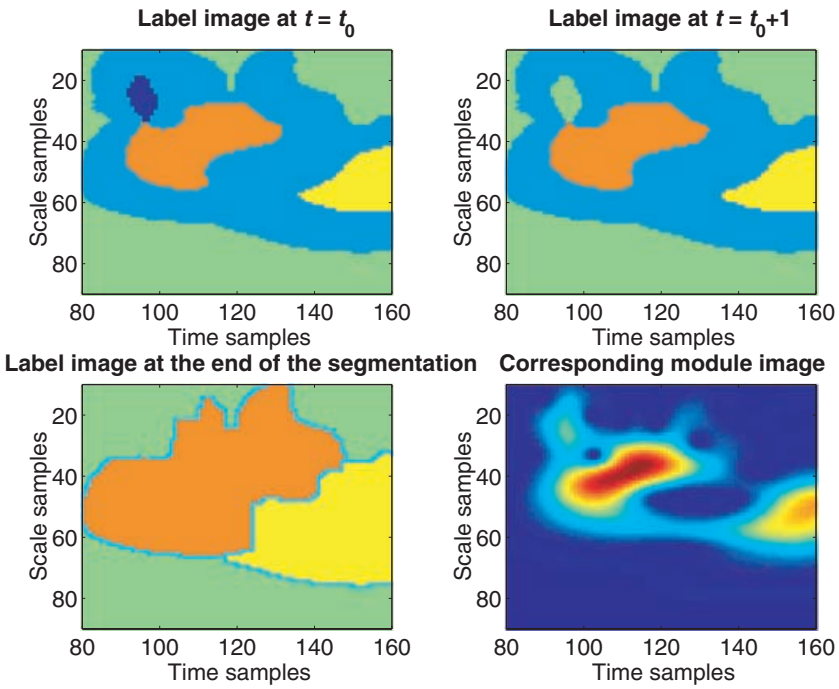

Figure 10 Rejection of the unexpected waves.

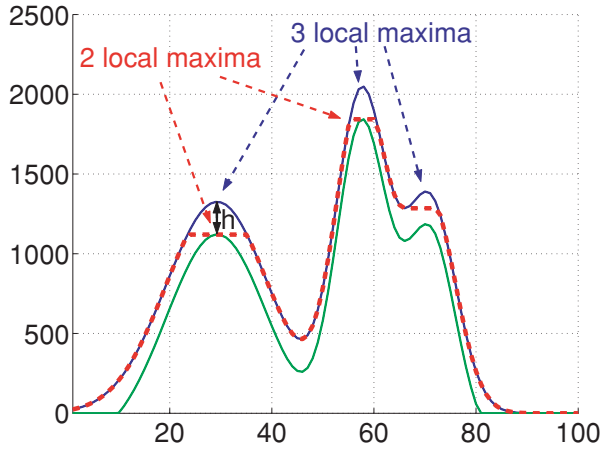

Figure 11 Illustration of the h_{max} transformation. The initial curve is in blue: it has three local maxima, theoretically leading to three different regions. The decreased curve is in green, and at the output of the geodesic reconstruction, we get the red curve where only two local maxima are present. The local maximum having a local contrast smaller than h_{max} has been removed.

dimensions (i.e. how the seeds are determined for each image) is explained.

4 TRACKING OF THE SEEDS OF THE SEGMENTATION

Let us recall that the profile contains N signals (one per sensor). Therefore, there are N time-scale images to segment in order to reconstruct the seismic profiles associated with the different waves. Stacking these N modulus images leads to a 3D volume. (We tried to segment this volume directly using a natural extension of the watershed algorithm to the 3D case. However, it turned out that it was not appropriate. Since the local extrema corresponding to the same wave were not connected from one image to another, the method led to an over-segmentation.) Figure 12 shows a thresholded representation (i.e. small values are not shown) of this volume: the perspective shows the different propagations from the background (corresponding to the sensor closest to the explosion) towards the reader. Four main 'tubes' can be seen; they correspond to the different waves of the profile (Fig. 1): from right to left, they are the slow Rayleigh wave, the fast Rayleigh wave, the reflected wave and the direct wave.

As illustrated in Fig. 12, since these waves propagate at different velocities, they will be more easily separated in the last trace (corresponding to the sensor furthest from the explosion). Consequently, the process is initialized on the last trace: the geophysicist indicates on the modulus image one maximum for each spot corresponding to a wave he wants to extract. This step initializes the algorithm. Note that this first seed estimation can also be done automatically: recall that the h_{max} transformation removes the maxima due to the noise (section 3.3); the remaining local maxima (which are the most significant) are the ideal seeds for the segmentation process. (If h_{max} is too low, there may be some over-segmentation

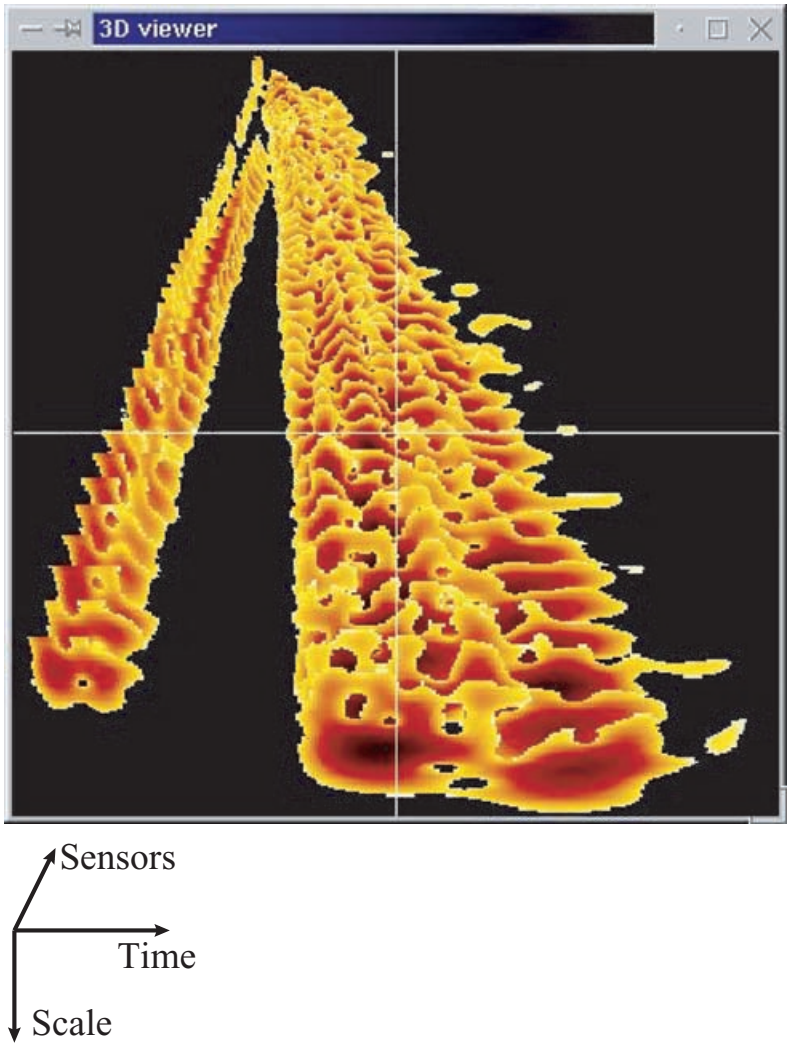

Figure 12 Forty-six time-scale planes stacked to form tubes.

due to the presence of irrelevant seeds, and if $h_{\max}$ is too high some lower energy waves may be considered as noise.) Nevertheless, the geophysicist usually likes to do this first step himself.

Then, using the continuity from one sensor to the next, the seeds (for each wave) can be tracked from one image to the other. Figure 13 shows two modulus images (denoted previous and next). The previous image is assumed to be already segmented. Then, to segment the next image, the seeds of all waves have to be estimated. We focus on the fast Rayleigh wave. It did not move fast on the time-scale plane (from the previous to the next modulus image). So the next seeds can be located at the highest values of the next modulus image which are in the green label of the previous label image. A thresholding isolates the highest green pixels. The same process is carried out for the other waves.

After many validations of this tracking process, it appeared that the results are perfect as long as the segmentation of the modulus image has been correctly carried out. If a bad segmentation occurs, the algorithm may not be stable enough to recover the good seeds for the next image. This issue will occur when the waves interfere on the time-scale plane. If two waves are quite close to each other, then their patterns overlap, and the modulus image does not represent two separate patterns: sometimes only one pattern can be seen for two waves. Then the segmentation cannot separate the waves perfectly. It can only cut the pattern into two pieces.

The 'previous modulus image' and the 'next modulus image' in Fig. 13 are fairly representative of these interference issues. On the first image, what we called the fast Rayleigh wave appears as a single convex pattern, whereas on the second image, the pattern has two energy domes which can be interpreted as

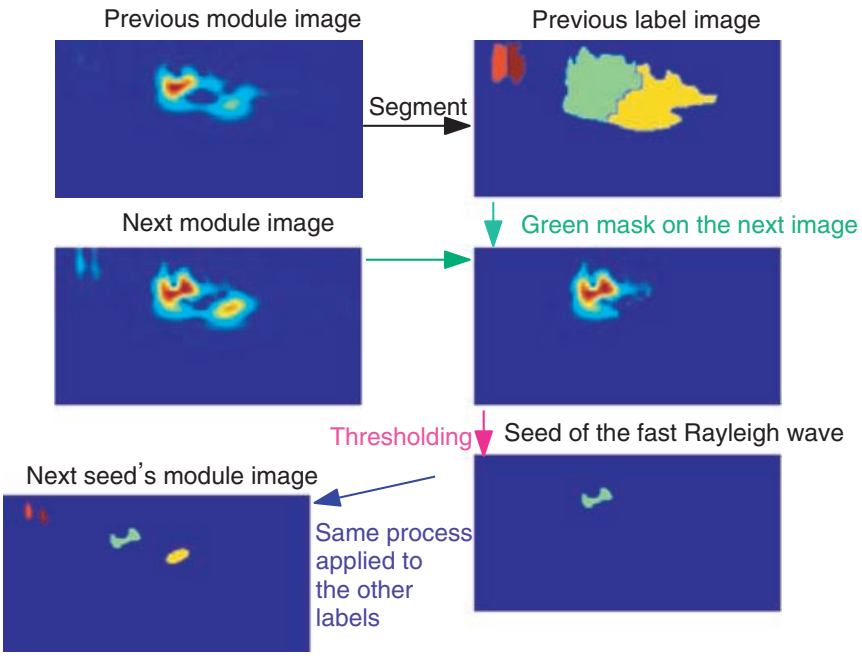

Figure 13 New seeds estimation.

the presence of two waves. The hidden wave may be the previously mentioned air wave (section 3.2). The change of pattern is due to the different phase wrapping from one trace to the other. Check that the holes caused by the interferences moved from (100, 30) on the first image, to (103, 28) on the second one. The algorithm presented does not solve the issue of interfering waves. If both interfering waves have almost the same amplitude (which means their associated local maxima have the same value), then the algorithm will merge both waves. On the other hand, the algorithm will reject the interfering wave whose amplitude is much lower. The decision is determined by the value of the threshold which characterizes the size of the seeds.

This shows that the algorithm cannot separate waves when they overlap in the time-scale plane.

5 RESULTS

The algorithm has been tested on different real data sets provided by the Geophysics Department (F. Glangeaud, LIS) and oil companies. The results obtained on the seismic profile of Fig. 1 are now presented. The tubes that can be seen on Fig. 12, which represent the stacking of the modulus images, have been separated by our algorithm (see Fig. 14). Then using the IWT, the different profiles have been reconstructed (see Fig. 15). The results are quite satisfactory and as good as those obtained by Nguyen *et al.* (1999): the 'tubes' have been correctly segmented, and the waves have been correctly separated and reconstructed. In addition these results have been positively validated by geophysicists. We must emphasize that the whole process is now automatic. The only problem which appears in these results is when the reflected wave is hidden by the fast Rayleigh wave. In this case, the reflected wave is no longer visible in the time-scale plane and other separation techniques must then be applied before or after this first process.

Similar tests have been carried out on other types of data: PSV, tubes waves, Love waves, etc., and these also led to positive validations. Figure 16 shows the results obtained in the case of a Love-wave extraction.

The errors that occur in the separation process are not due to the segmentation, which is robust, but to the bad representation of the modulus image, caused by interference between the different waves.

6 CONCLUSION

The watershed algorithm emerged as a powerful tool to segment time-scale images of seismic signals. The proposed method, which is unsupervised and almost non-parametric, leads to a robust and accurate wave separation. It segments all scalogram images and tracks the different waves from one trace to the next. Extra processing has been developed in order to address the problem of overlapping in the time-scale plane using polarization information (Roueff, Chanussot and Mars

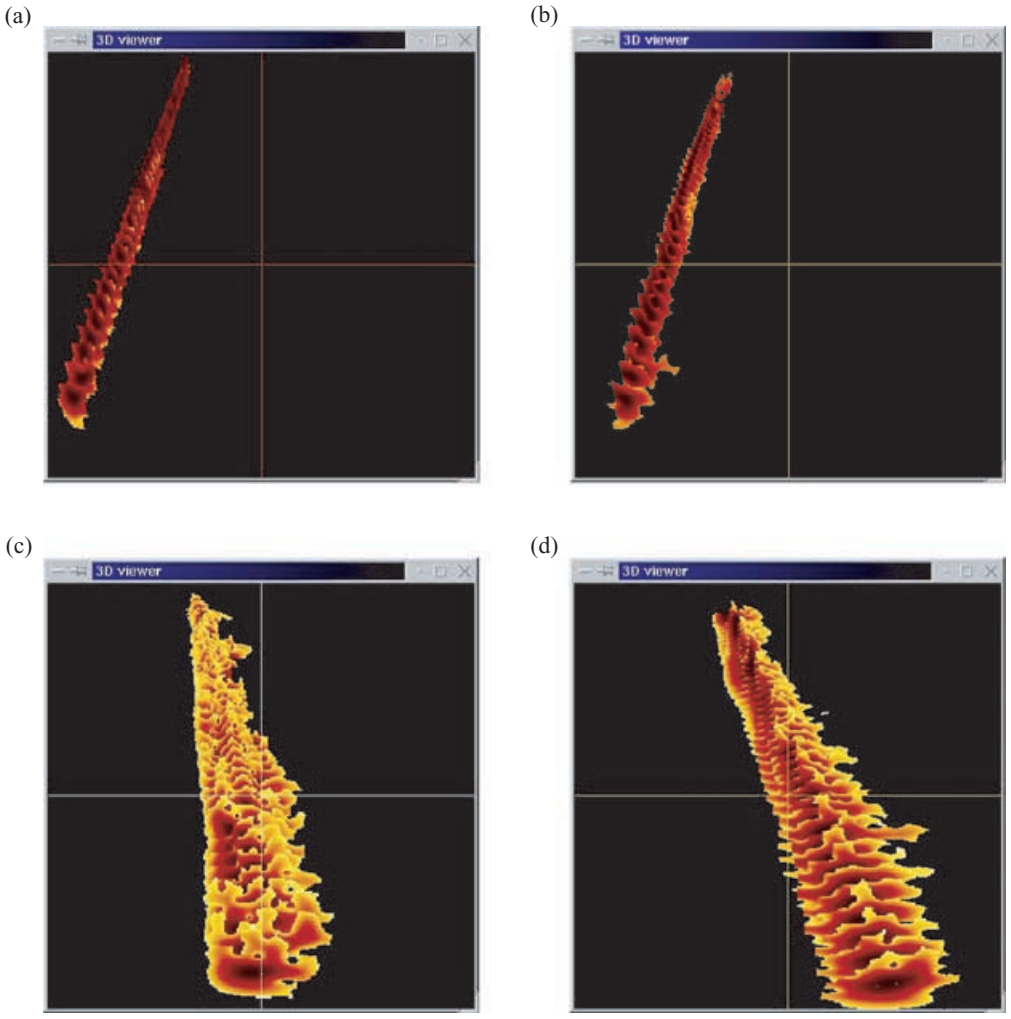

Figure 14 Forty-six time-scale planes stacked after separation. (a) Direct wave, (b) reflected wave, (c) fast Rayleigh wave, (d) slow Rayleigh wave.

2002) and velocity information (Roueff *et al.* 2003). However, this requires more intervention from the geophysicist.

Having an automatic separation process is an important feature when dealing with large amounts of data. In addition, the proposed separation in the time-scale plane is more efficient than the classical manual muting process. A perspective of this work is to adapt the tracking of the seeds to other kinds of data, e.g. multicomponent data, two-dimensional array data, etc.

ACKNOWLEDGEMENTS

The authors thank Michel Dietrich from the Laboratoire de Géophyisque Interne et de Tectonophysique (LGIT), and François Glangeaud and Barbara Nicolas from the LIS for their help.

REFERENCES

Abry P. 1997. *Ondelettes et Turbulences*. Diderot Multimedia.

Chakraborty A. and Okaya D. 1995. Frequency-time decomposition of seismic data using wavelet-based methods. *Geophysics* **60**, 1906–1916.

Chassande-Mottin E. 1998. *Méthodes de réallocation dans le plan temps-fréquence pour l'analyse et le traitement de signaux non stationnaires*. PhD thesis, Université de Cergy-Pontoise.

Daubechies I. 1992. *Ten Lectures on Wavelets*. SIAM.

Deighan A.J. and Watts D.R. 1997. Ground-roll suppression using the wavelet transform. *Geophysics* **62**, 1896–1903.

Gabor D. 1946. Theory of communication. *Journal of IEEE* **93**, 429–457.

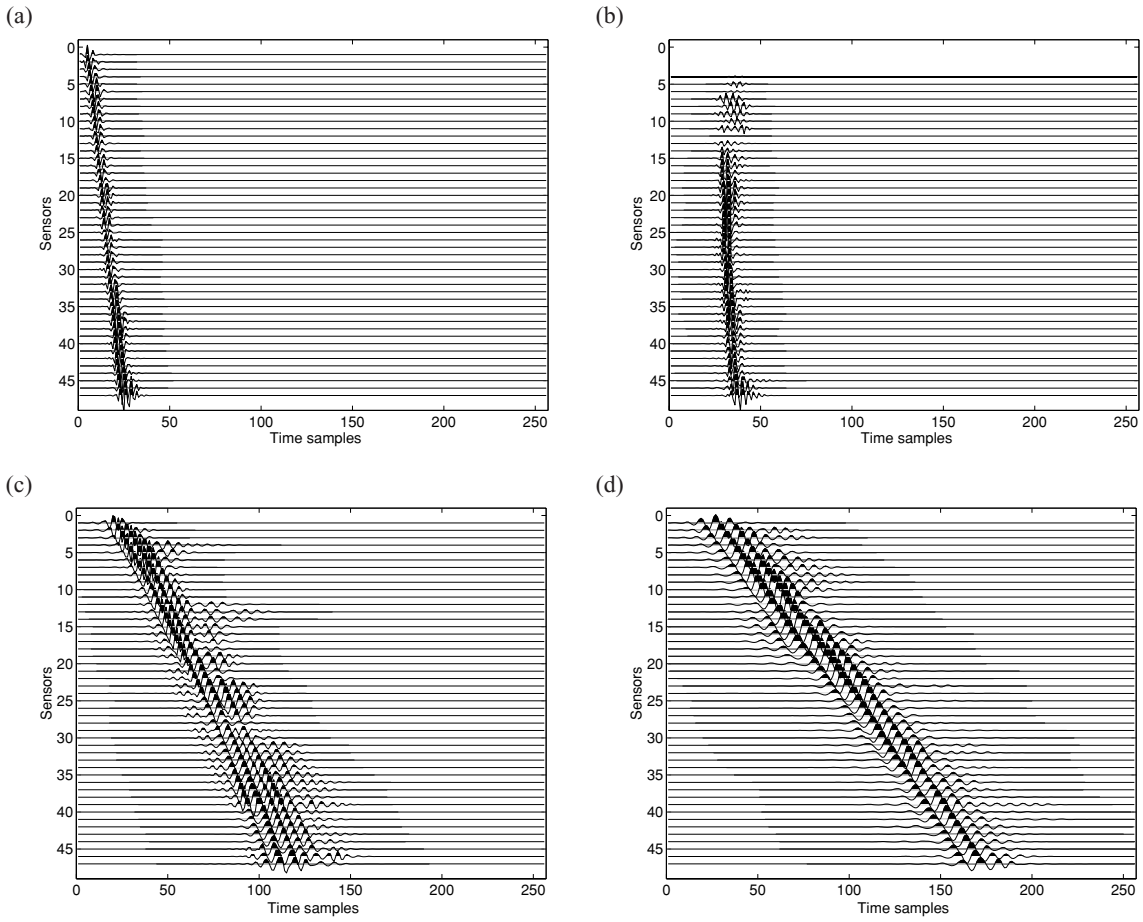

Figure 15 Seismic profiles of the different waves after separation by CWT and the automatic watershed algorithm. (a) Direct wave, (b) reflected wave, (c) fast Rayleigh wave, (d) slow Rayleigh wave.

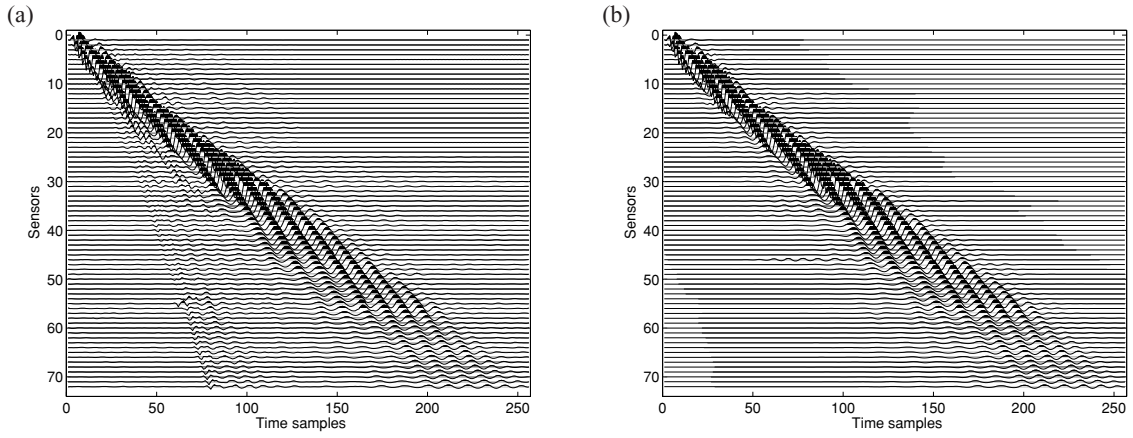

Figure 16 Love-wave extraction. (a) Initial profile, (b) profile of the extracted Love wave.

Kozek W. and Hlawatsch F. 1992. A comparative study of linear and nonlinear time-frequency filters. *Proceedings of the IEEE-SP International Symposium*, pp. 163–166.

Mari J.L., Glangeaud F. and Coppens F. 1999. *Signal Processing for Geologists and Geophysicists*. Ed. Technip, Paris.

Mars J., Rector J.W. and Lazaratos S.K. 1999. Filter formulation and wavefield separation of cross-well seismic data. *Geophysical Prospecting* **47**, 611–636.

Nawad S. and Quatrieri T. 1988. *Advanced Topics in Signal Processing*, Ch. Short-time Fourier transform. Prentice–Hall, Inc.

Nguyen M. 2000. *Analyse multi-dimensionnelle et analyse par ondelettes des signaux sismiques*. PhD thesis, Institut National Polytechnique de Grenoble.

Nguyen M.Q., Glangeaud F. and Mars J. 1999. Mixed surface waves elimination. 61st EAGE conference, Helsinki, Finland, Extended Abstracts, session 6021.

Papoulis A. 1977. *Signal Analysis*. McGraw–Hill Book Co.

Parker J.R. 1997. *Algorithms for Image Processing and Computer Vision*. John Wiley & Sons, Inc.

Pierson V. and Martin N. 1995. Watershed segmentation of time-frequency images. *Proceedings of IEEE Workshop on Non-Linear Signal and Image Processing (NSIP'95), Haldikiki, Greece*, pp. 1000–1003.

Roueff A., Chanussot J. and Mars J.I. 2002. Estimation of polarization on time-scale plane for seismic wave separation. *11th European Signal Processing Conference (EUSIPCO'02), Toulouse, France*, pp. 29–32.

Roueff A., Chanussot J., Nicolas B. and Mars J. 2001. Unsupervised seismic wave separation in the time-scale plane. 63rd EAGE conference, Amsterdam, The Netherlands, Extended Abstracts, 161–164.

Roueff A., Pedersen H., Mars J.I. and Chanussot J. 2003. Simultaneous group and phase correction for the estimation of dispersive propagating waves in the time-frequency plane. *International Conference on Acoustic Speech and Signal Processing (ICASSP'03), Hong-Kong*, pp. 429–432.

Serra J. 1988. *Mathematical Morphology*. Academic Press, Inc.

Vincent L. and Soille P. 1991. Watersheds in digital spaces: An efficient algorithm based on immersion simulation. *IEEE Transactions on Pattern Analysis and Machine Intelligence* **13**, 583–598.